Inorganic Chemistry

Open Access
This article is licensed under CC-BY 4.0

pubs.acs.org/IC
Article

Investigation of the La−Al−H and La−Si−H Systems at High Pressures

Doreen C. Beyer, Pedro Nunes Ferreira, Roman Lucrezi, Luiz Tadeu Fernandes Eleno, Holger Kohlmann, Christoph Heil, Michael Sannemo Targama, Volodymyr Baran, Shrikant Bhat, Robert Farla, Kristina Spektor, and Ulrich Häussermann*

Cite This: https://doi.org/10.1021/acs.inorgchem.5c05140

Read Online

ACCESS | Metrics & More | Article Recommendations | Supporting Information

ABSTRACT: Hydrogenation at gigapascal pressures can produce hydrides with potential superconducting, ionic, and hydrogen-storage properties. We studied the La−Al−H and La−Si−H systems up to 20 GPa using structure prediction and *in situ* synchrotron diffraction. In La−Al−H, only rhombohedral $LaAlH_6$ is stable. The La−Si−H system forms an orthorhombic monohydride, LaSiH, at low pressure, while $LaSiH_2$ and $LaSiH_7$ are predicted to be stable at 20 GPa, and $LaSiH_6$ is slightly unstable. $LaSiH_2$ is structurally related to the monohydride, whereas $LaSiH_6$ and $LaSiH_7$ feature SiH_6^{2-} units characteristic of hydridosilicates. Calculations predict superconductivity in $LaSiH_2$ and $LaSiH_6$ with $T_c \approx 10$ and 6 K. Experimentally, $LaSiH_2$ formation is indicated at 20 GPa, but higher hydrides were not observed due to decomposition into LaH_3 and Si, suggesting that pressures above 20 GPa are required to stabilize these phases at synthesis temperatures.

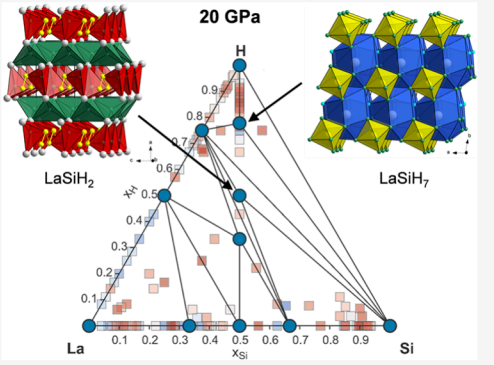

1. INTRODUCTION

The lanthanum−hydrogen system has attracted significant attention following the report of near room temperature superconductivity in LaH_{10} at pressures above 150 GPa.[1,2] Subsequent studies elaborated on this finding[3] and stimulated the investigation of numerous other *M*−H systems (e.g., M = Ca, Ce) from which a larger class of potentially high temperature superconducting (HT_c) hydrides emerged.[4−7] Yet these so-called superhydrides are only observable *in situ* at highly extreme conditions and as minute samples, which makes their characterization extremely challenging.[8] Comprehensive and conclusive studies of the HT_c phenomenon and, importantly, its potential exploitation as useful materials property would require that superhydrides can be retained as larger sample quantities at lower pressures, ideally at ambient pressure.[9,10]

With LaH_{10} as the starting point, design principles for robust ternary derivatives with HT_c properties have been suggested,[11,12] with the term "robust" referring to dynamic stability at pressures considerably lower than required for thermodynamic stability.[13,14] Dynamic stability indicates that a structure is in a local minimum of the potential energy surface. To actually retain a superhydride at low pressures would also require its kinetic stability toward decomposition into more stable configurations, i.e., sufficiently high potential energy barriers. Compared to binaries, ternary/multinary materials are expected to possess higher kinetic stability because of more complex decomposition pathways.[15] From theoretical works, $LaBH_8$ has been identified as dynamically stable down to 40 GPa and with a T_c of 126 K at 50 GPa.[13] For $LaBeH_8$, dynamic stability was calculated even down to 20 GPa, but experiments showed kinetic stability only to 80 GPa (at which $LaBeH_8$ displays a T_c of 110 K).[16] LaB_2H_8 has been shown kinetically stable down to 60 GPa and with a T_c of 106 K at 90 GPa.[17] Ultimately, for obtaining useful sample quantities for conclusive property characterization, it will be important to identify materials that are also thermodynamically stable at pressures down to 20−30 GPa.[9]

Against this background, we pursued an investigation of the La−Al−Si and La−Si−H systems by crystal structure prediction (CSP) and performed *in situ* studies of hydrogenations of the intermetallic samples LaAl, LaSi, and $LaAl_{0.5}Si_{0.5}$ at pressures up to 20 GPa. For this, we employed large volume press (LVP) high pressure methodology.[18] In contrast with diamond anvil cell (DAC) devices, pressures in LVP hydrogenations are limited to 20−25 GPa (and thus LVP techniques would not allow for the synthesis of LaH_{10}). In exchange, sample volumes are drastically increased (to tens of mm^3) and reaction environments at high *p*, *T* can be stably

Received: November 2, 2025
Revised: January 5, 2026
Accepted: January 13, 2026

Downloaded via DEUTSCHES ELEKTRONEN-SYNCHROTRON on January 27, 2026 at 10:47:52 (UTC).
See https://pubs.acs.org/sharingguidelines for options on how to legitimately share published articles.

© XXXX The Authors. Published by American Chemical Society

Table 1. Compilation of Performed Experiments and Applied Conditions

run	precursor	target pressure, GPa	T_{max}, °C	total heating duration, h	H content, assembly
#1, BT829	LaAl	10.2 → 12.1	490−495 → 630	~4.8	×8H, 14/7
#2, BT832	LaAl	2.2	490	~4.5	×8H, 14/7
#3, BT652	LaSi	9.0	570	~5.14	×6H, 14/7
#4, BT830	LaSi	20.0	800	~4.9	×8H, 10/4
#5, BT831	$LaAl_{0.5}Si_{0.5}$	9.3	615	~6.9	×8H, 14/7

maintained and well controlled over prolonged periods of time. We find that LaAl can be hydrogenated to $LaAlH_6$ at very low pressures, 2 GPa, and that $LaAl_{0.5}Si_{0.5}$ decomposes to $LaAlH_6$ + Si. CSP suggests thermodynamic stability for the previously unknown hydrides $LaSiH_2$ and $LaSiH_7$ at 20 GPa. The former material corresponds to a metal with a predicted T_c of around 10 K, whereas $LaSiH_7$ represents a semiconducting hydridosilicate with SiH_6^{2-} complexes. However, hydrogenation of LaSi at 20 GPa and temperatures around 500 °C resulted in decomposition to LaH_3 + Si, suggesting that higher pressures (outside the reach of LVP techniques) are needed for stabilizing these hydrides at synthesis temperatures.

2. EXPERIMENTAL AND COMPUTATIONAL DETAILS

2.1. Precursor Synthesis and Characterization

All steps of synthesis and preparations for sample characterization were carried out in a glovebox under an Ar atmosphere. Precursors with (nominal) compositions LaAl, LaSi, and $LaAl_{0.5}Si_{0.5}$ were prepared by arc melting 1−5 g batches of stoichiometric amounts of constituting elements (La, Chempur with a purity of 99.9% or better; Si, ABCR GmbH, 99,9999%; Al shots, ABCR GmbH, 99.999%). The samples were flipped over and remelted several times to ensure homogeneity. The total mass loss was negligible (<0.4 wt %). The obtained materials did not show noticeable degradation when exposed to air. The LaSi precursor corresponded to almost phase pure intermetallic compound LaSi with the orthorhombic FeB structure (*Pnma*),[19] whereas LaAl and $LaAl_{0.5}Si_{0.5}$ represented multiphase mixtures (LaAl, $LaAl_2$, La_5Al_4, La_2Al and $LaAl_{0.45}Si_{0.55}$, $La(Al_{0.88}Si_{0.12})_2$, $La_5(Al_{0.81}Si_{0.19})_4$, respectively) with an overall composition close to the nominal synthesis composition. For simplicity, we refer to these precursors in the following as LaAl and $LaAl_{0.5}Si_{0.5}$. See Supporting Information for details on the analysis of the precursor materials.

2.2. High Pressure Experiments and Data Analysis

All steps of sample preparation and recovery were performed in a glovebox under an Ar atmosphere. Powdered LaAl, LaSi, and $LaAl_{0.5}Si_{0.5}$ were compressed into pellets with a diameter of 1.0 mm and a height of 0.6−0.8 mm. In LVP hydrogenation, H_2 has to be delivered by a chemical source, which is integrated in the sample and releases H-fluid at the targeted *p*, *T* conditions.[18] Ammonia borane, BH_3NH_3, has emerged as preferred H-source as it possesses a high H content and decomposes neatly to inert BN and H_2 at high pressures.[20] The amount of BH_3NH_3 (ABCR, 97%) used for each sample corresponded to a molar ratio H_2:La of at least 3:1 (cf. Table 1). Precursor sample pellets were sandwiched between pelletized BH_3NH_3 and sealed inside NaCl capsules with 3.0 mm (14/7) or 2.5 mm (10/4) OD, according to established procedures.[21−23]

In situ high pressure experiments were performed at approximately 2 and 10−12 GPa for LaAl, 9 and 20 GPa for LaSi, and 9 GPa for $LaAl_{0.5}Si_{0.5}$ (cf. Table 1) and utilized the standard multianvil assemblies employed at the LVP beamline P61B, PETRA III, DESY (14/7 and 10/4 for pressures below and above 15 GPa, respectively).[24] For 10/4 assemblies, a 4.8 mm high TiB_2 heater (3.2 mm OD/2.5 mm ID), ZrO_2 with 3.2 mm OD, and NaCl capsules and MgO plugs with 2.5 mm OD were employed. Assemblies were compressed to target pressure and initially heated to a temperature between 250 and 350 °C at which the H-source BH_3NH_3 is expected to decompose and release hydrogen fluid.[20] The samples were then equilibrated for about 15−20 min before further heating. The temperature was evaluated from the power-*T* calibration curves. Energy-dispersive XRD (EDXRD) patterns were collected using two germanium solid-state detectors positioned at around 3 and 5°, respectively. Angle calibration was performed using LaB_6 SRM 660c. Initial data evaluation and manipulation utilized PDIndexer.[25] The Le Bail analysis[26] of the *in situ* EDXRD data was performed in GSAS-II.[27] Pressure was estimated from reflections of the sample capsule and using the equation of state of NaCl by Matsui et al.[28]

2.3. *Ex Situ* PXRD Characterization of La−Al/Si−H Products

The products obtained from runs #1, #3, and #5 were recovered in a glovebox under an argon atmosphere. Approximately half of each sample pellet was sealed inside a 1.0 mm wide glass capillary. PXRD patterns were collected at the beamline P02.1, PETRA III, DESY[29] using monochromatic synchrotron radiation (λ = 0.20730 Å, $E \approx 60$ keV) at ambient *p*, *T*. Data was collected on spinning samples (~5000 Hz) using the Varex XRD 4343CT (150 × 150 μm^2 pixel size, 2880 × 2880 pixel area) detector and integrated using the pyFAI software.[30] Calibration was performed based on data collected for LaB_6 powder (SRM 660c). For indexing of the angle-dispersive powder patterns, the DICVOL[31] and TAUP algorithms[32] within the CRYSFIRE package were used.[33] Rietveld refinements[34] of the *ex situ* PXRD data were performed in Fullprof.[35] Formation of lanthanum hydride was observed during the experiments. Since in all the experiments a H_2:La ratio of at least 3:1 was employed, a stoichiometric formation of LaH_3 was assumed.[36] With the techniques used, LaH_3 could not clearly be distinguished from a mixed stoichiometry LaH_{2+x} ($0 \leq x \leq 1$). For Rietveld refinements of the recovered samples, a $Fm\bar{3}m$ LaH_3 structure was used.

2.4. Theoretical Calculations

The USPEX package[37,38] was employed for evolutionary CSP to sample the phase space of possible candidate structures in the ternary systems of La−Al−H and La−Si−H. For each pressure, 0 and 20 GPa, several independent USPEX runs were performed with variable composition (VC) according to (i) the binary boundary lines La−Al, La−Si, Si−H, Al−H, and La−H, (ii) the full ternary space, and (iii) the pseudobinary lines LaSi−H and LaAl−H. All VC runs were restricted to unit cells containing 16−32 atoms. Additional fixed-composition (FC) runs were performed at 0 and 20 GPa for the stable or nearly stable compositions determined in the VC runs: LaSiH, $LaSiH_6$, and $LaSiH_7$. For each FC, we carried out three separate runs with the number of atoms per cell restricted to 6−12, 12−24, 24−48 for LaSiH; 8−16, 16−32, and 24−48 for $LaSiH_6$; 9−18, 18−36, 27−54 for $LaSiH_7$. For the composition of $LaSiH_2$, no stable structure was found within the VC runs and two candidates, determined by chemical intuition, were added by hand. Within the described USPEX runs, we sampled a total of approximately 10,000 (15,000) structures per pressure for the ternary La−Al−H (La−Si−H) systems.

The geometry optimization (relaxation) of suggested candidate structures, as well as the calculation of energies, forces, and stress tensors, were carried out within density-functional theory (DFT) as implemented in the VASP code,[39,40] using projector-augmented-wave (PAW)[41] pseudopotentials and the Perdew−Burke−Ernzerhof (PBE)[42] exchange-correlation functional. For each structural relaxation, we employed a five-step procedure with gradually increasing numerical parameters and convergence criteria, up to a final step with an energy cutoff for the plane-wave basis set of 375 eV,

https://doi.org/10.1021/acs.inorgchem.5c05140
Inorg. Chem. XXXX, XXX, XXX−XXX

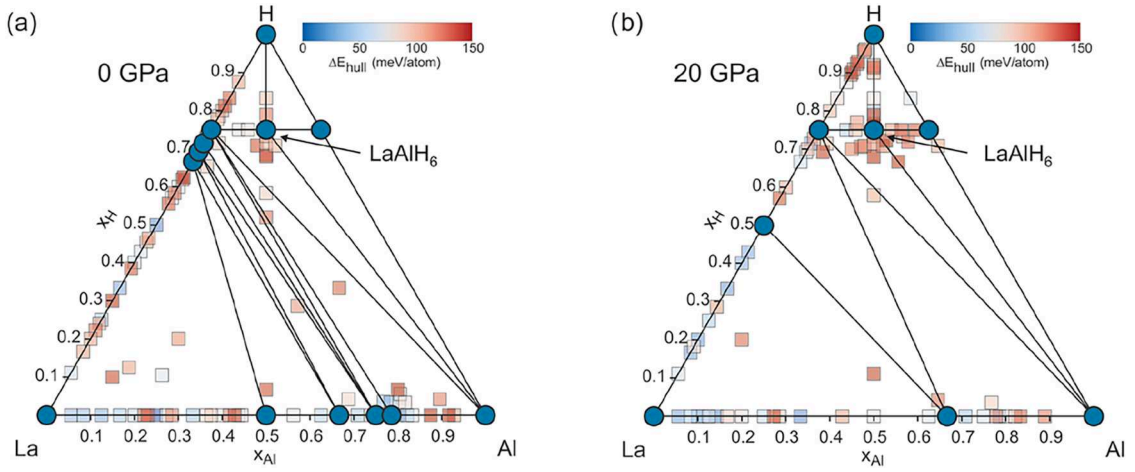

Figure 1. La−Al−H ternary phase diagram according to CSP at 0 (a) and 20 GPa (b). Blue circles represent compounds located on the convex hulls. Square symbols denote phases above the convex hulls. The colors of the squares (ranging from blue to red) indicate the magnitude of instability.

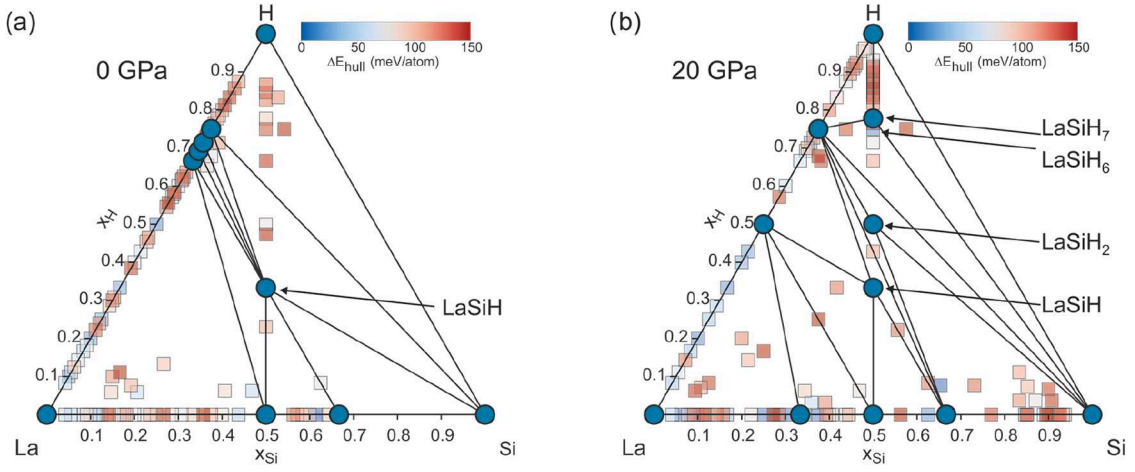

Figure 2. La−Si−H ternary phase diagram according to CSP at 0 (a) and 20 GPa (b). Blue circles represent compounds located on the convex hulls. Square symbols denote phases above the convex hulls. The color of the squares (ranging from blue to red) indicates the magnitude of instability.

a **k**-grid spacing of 0.04 2π Å^{-1}, a smearing value of 0.06 eV, and a self-consistency threshold of 10^{-6} eV.

For selected structures, we performed additional DFT calculations via the Quantum ESPRESSO (QE) package.[43−45] Vibrational properties and electron−phonon coupling quantities were calculated within density-functional perturbation theory (DFPT).[47] We used scalar-relativistic optimized norm-conserving Vanderbilt (ONCV) pseudopotentials from the SG15 ONCV library[46,48] in combination with the PBE[42] exchange-correlation functional. The kinetic energy cutoff for the wave functions was set to 100 Ry, the **k**-grid spacing to 0.02 2π Å^{-1}, the convergence threshold for the electronic self-consistency to 10^{-10} Ry, and a Methfessel-Paxton smearing[49] value of 0.01 Ry was used for metallic structures. These settings provide a numerical accuracy for the total energy of well below 1 meV/atom with respect to selected reference calculations with an energy cutoff of 300 Ry and a **k**-grid spacing of 1/3 0.02 2π Å^{-1}. The Henkelman-group approach and code[50−52] was used for the Bader analysis.[53] The required charge-densities were calculated using kjPAW[54] pseudopotentials from the PSLibrary[55] employing a kinetic energy cutoff of 140 Ry for the wave functions and 1120 Ry for the charge-density.

The phonon self-consistency threshold was set to 10^{-16}, and the employed **q**-grids were 4 × 4 × 4 for LaSiH and LaSiH$_6$, 2 × 4 × 4 for LaSiH$_2$, and 2 × 2 × 2 for LaSiH$_7$. The electron−phonon matrix elements were integrated over a denser **k**-grid with spacing of 0.01 2πÅ^{-1} and for 20 double-delta smearing values in the range of 0.002−0.040 Ry, where a value of 0.010 Ry was chosen for the presented results in combination with a phonon smearing value of 0.2 THz for the **q**-grid integration. Based on the obtained Eliashberg spectral function $\alpha^2F(\omega)$, the electron−phonon coupling strength λ and the logarithmic average phonon frequency ω_{log} are calculated according to

$$\lambda(\omega) = 2\int_0^{\omega} d\omega' \frac{\alpha^2F(\omega')}{\omega'}$$

with $\lambda = \lambda(\infty)$ and

$$\omega_{log} = \exp\left(\frac{2}{\lambda}\int_0^{\infty} d\omega \frac{\alpha^2F(\omega)\ln\omega}{\omega}\right)$$

The T_c values are obtained by solving the isotropic Migdal-Eliashberg (ME) equations in the full-bandwidth formulation using the IsoME package[56] and a typical value for the Morel-Anderson pseudopotential[57] of $\mu^* = 0.1$ (specified as μ^{AD} in IsoME).

3. RESULTS AND DISCUSSION

3.1. Crystal Structure Prediction (CSP)

The results from CSP for the ternary systems La−Al−H and La−Si−H for 0 and 20 GPa are compiled in Figures 1 and 2,

https://doi.org/10.1021/acs.inorgchem.5c05140
Inorg. Chem. XXXX, XXX, XXX−XXX

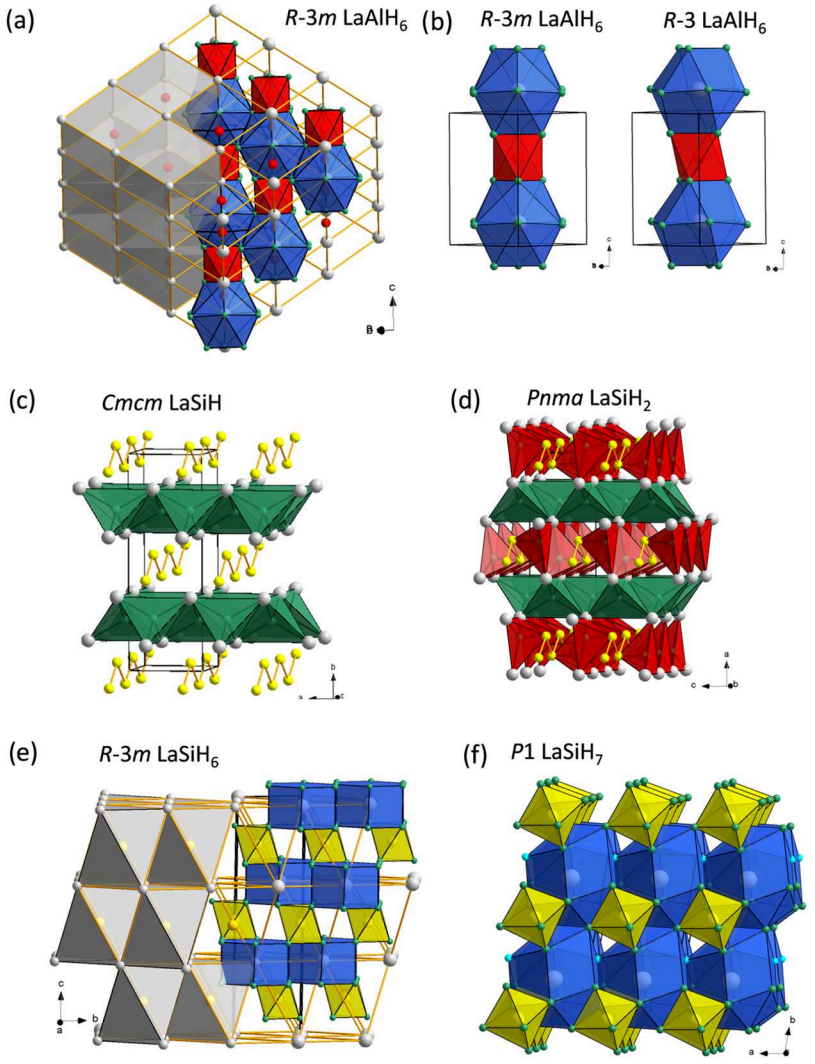

Figure 3. (a) Crystal structure of $R\bar{3}m$ $LaAlH_6$, highlighting the CsCl-type arrangement of La^{3+} and AlH_6^{3-} ions. The cuboctahedral and octahedral coordination for La and Al by H atoms, respectively, are shown as blue and red polyhedra. (b) Comparison of the arrangement of LaH_{12} and AlH_6 polyhedra in $R\bar{3}m$ and slightly more stable $R\bar{3}$ $LaAlH_6$. (c) Crystal structure of the interstitial hydride *Cmcm* LaSiH, which closely relates to the CrB structure type. Tetrahedral interstitials defined by 4 La atoms and filled by H atoms are depicted as green polyhedra. (d) Crystal structure of *Pnma* $LaSiH_2$. Compared to LaSiH, a second type of tetrahedral interstices defined by 3 La and 1 Si atoms is filled by H atoms (red polyhedra). (e) Rhombohedral crystal structure of metastable $LaSiH_6$, highlighting the NaCl arrangement of La^{3+} and SiH_6^{2-} ions. The hexagonal prismatic and octahedral coordinations for La and Si by H atoms, respectively, are shown as blue and yellow polyhedra. (f) Crystal structure of *P*1 $LaSiH_7$. La is coordinated irregularly by 14 H atoms (depicted as blue polyhedra).

respectively. For La−Al−H, only previously known $LaAlH_6$ is a stable ternary compound. The $LaAlH_6$ structure contains isolated $[AlH_6]^{3-}$ octahedra and was reported with a $R\bar{3}m$ structure ($BaSiF_6$ type),[58] Figure 3a. La and Al atoms form a rhombohedrally distorted CsCl structure, which implies that AlH_6^{3-} octahedra are surrounded by a rhombically distorted cube of La atoms. La atoms are 12-coordinated by H atoms in a cuboctahedral fashion. We find that a lower symmetric $R\bar{3}$ structure is more stable, very slightly at ambient pressure and increasingly with pressure. This is depicted in Figure S1. The symmetry lowering is shown in Figure 3b. It is considered unlikely that additional ternary La−Al−H hydrides can be synthesized at pressures accessible with LVPs; instead substantially higher pressures would be required. A superconducting solid solution $(La,Al)H_{10}$ being stable at 146 GPa has been recently reported.[59]

For La−Si−H at ambient pressure (Figure 2a), the interstitial hydride LaSiH with a *Cmcm* structure (Figure 3c) represents the only stable ternary compound. Also, this compound, although H-deficient, has been reported earlier.[60,61] $LaSiH_x$ with $x = 0.6–0.9$ was obtained as a dimorphic mixture of related *Cmcm* and *Pnma* phases in close to ambient pressure hydrogenations of LaSi.[61] According to DFT calculations, the *Cmcm* form is slightly more favorable, by around 18 meV/atom at ambient pressure, and remains so, although increasingly less with pressure, cf. Figure S2. LaSiH features polyanionic zigzag chains of Si atoms ($_\infty^1[Si^{2-}]$) and hydridic H (H^-) incorporated in tetrahedral La_4 interstices and may be formally considered as charge-balanced Zintl phase hydride $La^{3+}(Si^{2-})(H^-)$.[61]

The La−Si−H diagram at 20 GPa looks noticeably different by revealing additionally the stable hydrides $LaSiH_2$ and $LaSiH_7$ (Figure 2b). $LaSiH_2$ has a *Pnma* structure which resembles that of $BaSiH_2$.[62] This structure can be derived from *Cmcm* LaSiH by additional H occupying a second kind of tetrahedral interstice defined by three La atoms and one Si

https://doi.org/10.1021/acs.inorgchem.5c05140
Inorg. Chem. XXXX, XXX, XXX−XXX

atom (La_3Si), as shown in Figure 3d. In contrast with LaSiH, $LaSiH_2$ would not correspond to a charge-balanced compound. $LaSiH_7$ is a hydridosilicate. Its structure is depicted in Figure 3f. The characteristic of hydridosilicates is hypervalent octahedral SiH_6^{2-} moieties. $LaSiH_7$ appears charge-balanced due to the simultaneous presence of the H^- ion. Interestingly, the composition $LaSiH_6$ also seems feasible. A hydridosilicate with $R\bar{3}m$ structure (Figure 3e) is just slightly above the ternary hull (by 18 meV/atom), and thus could potentially be stable at finite temperatures or be accessible as a metastable phase.[63] Like $LaSiH_2$, $LaSiH_6$ would be charge-imbalanced and represent a metal.

Hydridosilicates have been recently established with alkali and alkaline earth metal counterions, e.g., K_2SiH_6, $BaSiH_6$, from high pressure hydrogenations at 4−10 GPa.[23,64−66] Hitherto, these materials have been exclusively found as charge-balanced, semiconducting compounds. Here, the CSP indicates a possible extension of hydridosilicates toward trivalent lanthanide counterions. In the $P1$ $LaSiH_7$ structure, La ions are irregularly coordinated by 14 H atoms. La ions and SiH_6^{2-} moieties attain a mutually tetrahedral coordination (relating to the wurtzite structure). In the $R\bar{3}m$ $LaSiH_6$ structure, La ions are hexagonal-prismatically coordinated by 12 H atoms. La ions and SiH_6^{2-} moieties are arranged as in the cubic NaCl structure, which is similar to the arrangement of constituents in $BaSiH_6$[66] but contrasts with the CsCl-like arrangement of La ions and AlH_6^{3-} moieties in the $LaAlH_6$ structure, see Figure 3a. The electronic structure and dynamic stability of the ternary $LaSiH_n$ compounds will be discussed in more detail in Section 3.3.

3.2. *In Situ* Experiments

3.2.1. LaAl. High pressure hydrogenations of LaAl were performed at 2 and 10−12 GPa. Figure 4 shows the evolution of EDXRD patterns during heating to 490 °C at 10 GPa, further compression to 12 GPa, and final heating to 630 °C. After hydrogen release at ∼300 °C and up to ∼355 °C, broad diffraction peaks in the energy range of 75−100 keV indicated the formation of intermediate hydride phases. At ∼390 °,C reflections of rhombohedral $LaAlH_6$ appeared. The phase was stable upon further heating to 490 °C at 10 GPa and up to 630 °C after further pressure increase to 12 GPa. After cooling and decompression, $R\bar{3}m$ $LaAlH_6$ was recovered to ambient conditions. Its PXRD pattern, shown in Figure 5, revealed the presence of a minute amount of LaH_3 (about 5% with respect to $LaAlH_6$), indicating the onset of decomposition above 600 °C and 12 GPa. Theory suggested that a less symmetric $R\bar{3}$ structure is more stable. Since the symmetry lowering essentially relates to the H atom arrangement, possibly only neutron diffraction (on deuterated samples) may reveal the actual structure of $LaAlH_6$.

$LaAlH_6$ was previously obtained from a mechanochemically assisted metathesis reaction between $LaCl_3$ and $NaAlH_4$, according to $LaCl_3 + 3NaAlH_4 \rightarrow LaAlH_6 + 3NaCl + 2Al + 3H_2$, using a 3× excess of $NaAlH_4$ and employing a slightly pressurized hydrogen atmosphere (1−15 bar).[58] The reaction produced side products (Al and NaCl) and required several hours for completion. Here, we obtained $LaAlH_6$ from direct synthesis by hydrogenating the intermetallic compound mixture "LaAl". Hydrogenation attempted at the lowest possible pressures, around 2 GPa, showed $LaAlH_6$ formation at 270 °C, see Figure S3. When heating to 490 °C, decomposition to LaH_3 + Al was observed. It may be possible

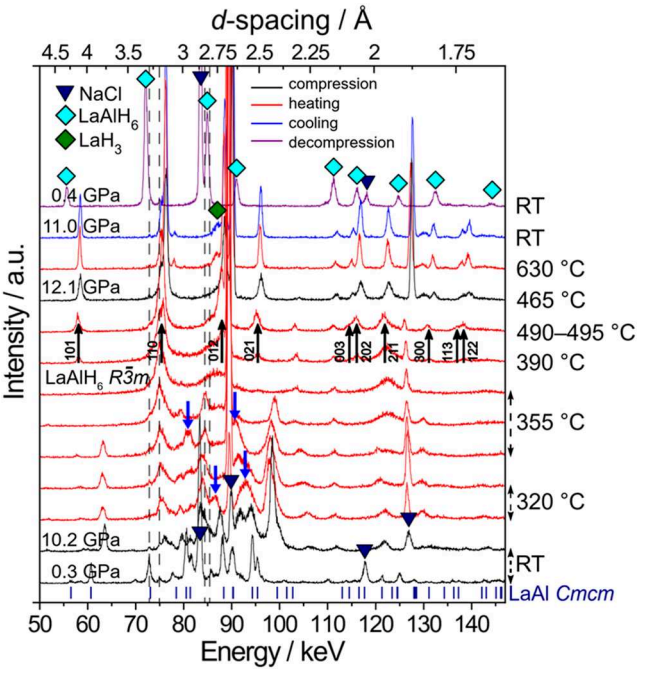

Figure 4. Hydrogenation of LaAl at 10−12 GPa. Diffraction patterns are shown for the starting and initial target pressure (10.2 GPa, black), during heating to 490 °C (red), further compression to 12.1 GPa (black), and further heating to 630 °C (red), after cooling to room temperature (blue), and after decompression (purple). Secondary Pb fluorescence peaks (from the detector shielding) are marked as dashed gray vertical lines, and blue triangles mark NaCl reflections from the sample capsule. The evolution of intermediate ternary hydride phases between hydrogen release at ∼320 °C and heating to 355 °C is indicated by blue arrows. The onset of $LaAlH_6$ formation at 390 °C is marked by black arrows.

that $LaAlH_6$ can also be synthesized by conventional autoclave hydrogenations using pressures 10−100 bar. The lattice parameters of $LaAlH_6$ at various p, T conditions are compiled in Table S1.

3.2.2. $LaAl_{0.5}Si_{0.5}$. High pressure hydrogenation of the $LaAl_{0.5}Si_{0.5}$ precursor was performed at about 9.3 GPa, Figure S4. An intermediate hydride $LaAl_{0.5}Si_{0.5}H_x$ (with $Cmcm$ structure and relating to LaSiH, cf. Figure 3c) may be inferred upon dwelling the sample at 320 °C, see Figure S5. The formation of $LaAlH_6$, obviously accompanied by the decomposition of $LaAl_{0.5}Si_{0.5}H_x$, was seen at 340 °C. After heating to 480 °C, LaH_3 peaks emerged. At 560 °C, the sample corresponded to a mixture of $LaAlH_6$, LaH_3, and Si. Figure S6 shows the Rietveld fit of the recovered sample. The lattice parameter of so obtained $LaAlH_6$ is virtually identical to the one obtained from LaAl hydrogenations, cf. Table S1, indicating that Si cannot substitute for Al in $LaAlH_6$.

3.2.3. LaSi. High pressure hydrogenations of LaSi were conducted at 9 and 20 GPa. The evolution of EDXRD patterns from the 9 GPa experiment upon heating is shown in Figure S7. At around 260 °C, after hydrogen release, reflections appeared that indicated the formation of a mixture of $Cmcm$ and $Pnma$ LaSiH. This would be similar to the outcome of earlier reported hydrogenations of LaSi at low (near ambient) pressure.[61] The Le Bail analysis of the 345 °C pattern, shown in Figure S8, provides a rather good fit. However, the $Cmcm$ model gives a too large volume compared to that of the DFT calculated $Cmcm$ LaSiH structure at the same pressure (cf.

https://doi.org/10.1021/acs.inorgchem.5c05140
Inorg. Chem. XXXX, XXX, XXX−XXX

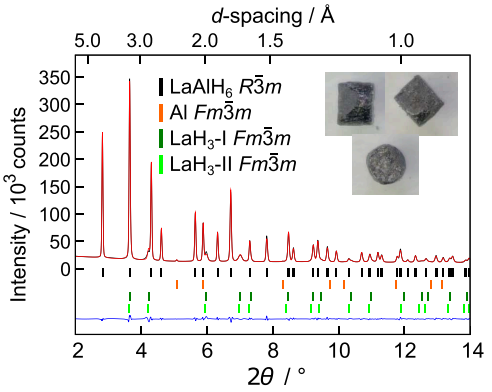

Figure 5. Rietveld fit to the synchrotron PXRD pattern (λ = 0.20734 Å, ambient conditions) of the product from the hydrogenation of LaAl at 10.2−12.1 GPa and 630 °C (cf. Figure 4). The inset shows photographs of the recovered sample (OD ∼ 1 mm). Lanthanum hydride reflections display an asymmetric peak shape. Refinement using two $Fm\bar{3}m$ structures resulted in a better fit, which could be attributed to a variable H content. Still, the phases are termed LaH_3−I and LaH_3−II for consistency. $LaAlH_6$ $R\bar{3}m$[52] (black): 85.2(3) wt %, Al $Fm\bar{3}m$ (orange): 1.6(1) wt %, LaH_3−I $Fm\bar{3}m$[36] (dark green): 8.7(1) wt %, LaH_3−II $Fm\bar{3}m$[36] (light green): 4.5(2) wt %. Lattice parameters $LaAlH_6$ $R\bar{3}m$: a = 6.51412(4) Å, c = 6.32682(6) Å, V = 232.502(3) Å^3 (R_{bragg} = 1.13%, R_f = 0.975%), LaH_3−I: a = 5.6231(2) Å, LaH_3−II: a = 5.656(3) Å. R_p = 2.20%, R_{wp} = 3.09%, R_{exp} = 0.67%.

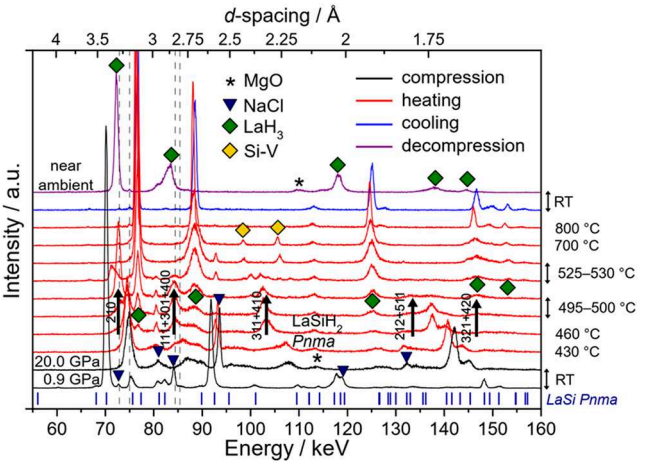

Figure 6. Hydrogenation of LaSi at 20 GPa. Diffraction patterns are shown for the starting and target pressure (black), during heating to 800 °C (red), after cooling to room temperature (blue), and after decompression (purple). Secondary Pb fluorescence peaks (from the detector shielding) are marked as dashed gray vertical lines. Green and yellow diamonds mark LaH_3 and hexagonal Si−V. Blue triangles mark NaCl reflections from the sample capsule and asterisks mark MgO from the pressure cell assembly. The formation of the hydride phase at 460−500 °C, tentatively assigned as *Pnma* $LaSiH_2$, is marked by black arrows. The origin of the peak at 137.5 keV, appearing at 460 °C and vanishing during dwelling at 495−500 °C, has not been identified. It is likely connected to the beginning of hydrogen uptake by the educt.

Figure S11). Thus, the extracted *Cmcm* phase may contain additional hydrogen or the reflections do not represent a phase mixture but an unknown (mono)hydride. At 440 °C, the appearance of LaH_3 reflections indicated onset of decomposition, which was completed at 470 °C. At the same time, a set of new reflections emerged, which could not be assigned or indexed. This phase (or phase mixture) is stable until 570 °C and seems to be recoverable at ambient pressure; see Figure S9.

At 20 GPa, the onset of hydrogenation was observed at 460 °C by the appearance of a set of broad reflections, see Figure 6 (note that the decomposition behavior of BH_3NH_3 at pressures above 10 GPa is not well studied, but presumably occurs at between 350−400 °C and only releasing 2 × H_2). Rather simultaneously with the emergence of broad hydride phase reflections, the formation of LaH_3 was noticeable, which indicates decomposition of the initial ternary hydride phase. At 495−500 °C and within 25 min dwell time, reflections from the LaSi precursor had vanished and hydride reflections grew more prominent. The LeBail fit of the 500 °C pattern after the dwell is shown in Figure S10. The hydride phase likely corresponds to the predicted *Pnma* $LaSiH_2$. The DFT calculated unit cell volume for *Pnma* $LaSiH_2$ at around 20 GPa (shown in Figure S11) would match rather closely the unit cell volume obtained from the LeBail fit of the 500 °C data. However, the quality of diffraction data is low and additionally obscured by the simultaneous presence of broad LaH_3 peaks. At 530 °C, $LaSiH_2$ decomposed completely to LaH_3 and Si with a simple hexagonal structure (Si−V). Lattice parameters for Si−V could be extracted via LeBail fitting using GSAS-II (530 °C: a = 2.5503(5) Å, c = 2.3755(5) Å, V = 13.380(4) Å^3; 700 °C: a = 2.5609(4) Å, c = 2.3773(4) Å, V = 13.501(3) Å^3). Melting of Si−V occurred between 700 and 800 °C, which is in agreement with the reported melting curve of Si (∼780 °C at 20 GPa).[67] After the sample is cooled to RT, Si is invisible in the EDXRD patterns. This is attributed to the formation of large Si grains after crystallization from the melt, producing spotty diffraction rings, which cannot be detected by the point detector. LaH_3 forms simultaneously with $LaSiH_2$ and its reflections continued to grow after decomposition of $LaSiH_2$. Some reflections display broadening, indicating a possible deviation from the cubic cell. Above 700 °C, they sharpen, suggesting a transition to cubic symmetry (at 800 °C: a ≈ 5.31 Å), which is retained on cooling to RT. This low symmetry distortion was not observed clearly in the lower pressure runs.

Although the formation of $LaSiH_2$ remains ambiguous and there is no evidence of $LaSiH_7$ in our experiment, we stress that CSP clearly indicates the stability of higher hydrides in La−Si−H at 20 GPa. In addition, phonon calculations show dynamic stability of $LaSiH_2$ and $LaSiH_7$ at 20 GPa (Figure S13) and also at ambient pressure (Figure S12), which strengthens the feasibility of their synthesis and, even more, their potential recovery at ambient pressure (although the kinetic stability of $LaSiH_2$ and $LaSiH_7$ at ambient pressure is uncertain). However, CSP is based on zero Kelvin calculations, whereas synthesis will require elevated temperatures for overcoming kinetic barriers. Assessing altered thermodynamic stability at finite temperature and kinetics for both formation and decomposition of hydride products, which often have different pathways, is computationally very expensive. The rather simultaneous formation of hydride and decomposition into LaH_3 and Si suggests that required synthesis/reaction temperatures are comparable to the decomposition temperature at 20 GPa and, consequently, higher pressures and/or a higher H_2 fluid activity would be needed. In this respect, we need to point out that the amount of H_2 (×8H) employed for this experiment may not have been sufficient for hydridosilicate formation since BH_3NH_3 decomposition at 20 GPa (most

https://doi.org/10.1021/acs.inorgchem.5c05140
Inorg. Chem. XXXX, XXX, XXX−XXX

likely) arrests at a polymeric "BHNH". Against this background, a closer look at the compounds $LaSiH_n$ is warranted.

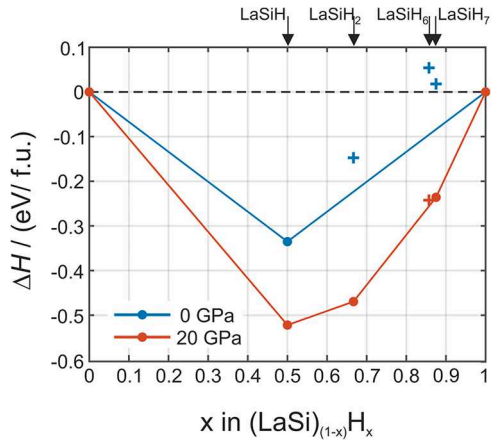

Figure 7. Convex hulls for the pseudobinary LaSi − H_2 line at 0 and 20 GPa (cf. Figure 3). Stable phases at 20 GPa (red circles) are *Cmcm* LaSiH, *Pnma* $LaSiH_2$, and *P*1 $LaSiH_7$. $R\bar{3}$ $LaSiH_6$ is above the hull by only 15 meV/atom (red cross). At 0 GPa, *Cmcm* LaSiH remains thermodynamically stable, whereas the higher hydrides (blue crosses) only retain dynamic stability, see phonon dispersions provided as Supporting Information, Figures S12 and S13, respectively.

3.3. The $(LaSi)_{1-x}H_x$ Pseudobinary Line

Figure 7 depicts the convex hulls of the pseudobinary line (LaSi−H_2) at 0 and 20 GPa, which are extracted from the data shown in Figure 2. These hulls reflect the stability of $LaSiH_n$ with respect to the reactants LaSi and H_2 or, alternatively, mirror the energetics of the formation reaction. With respect to the ternary hull, $LaSiH_6$ is more stable but still remains above the pseudobinary convex hull (by 15 meV/f.u.), which may be altered at a finite temperature. At ambient pressure, $LaSiH_2$, $LaSiH_6$, and $LaSiH_7$ appear rather unstable, by about 75, 150, and 100 meV/f.u., respectively (with respect to LaSiH and H_2). Yet these phases may be kinetically stable.

Figure 8 compares the electronic structures, band structures, and density of states (DOS) of LaSiH, $LaSiH_2$, $LaSiH_6$, and $LaSiH_7$ at their calculated equilibrium volumes, i.e., at 0 GPa. LaSiH appears metallic, although it formally corresponds to a charge-balanced Zintl phase $La^{3+}[Si]^{2-}(H^-)$, Figure 8a. The Fermi level is located in a pronounced pseudo gap in the DOS. Noticeably, a large contribution of La states to occupied bands, in agreement with an earlier analysis of the electronic structure of LaSiH.[61] According to the Zintl concept, $LaSiH_2$ is imbalanced, $La^{3+}[SiH]^-(H^-)e$. Its DOS (Figure 8b) has some resemblance to LaSiH, but at the same time, it deviates considerably from a rigid band behavior. The lowest lying bands, with mostly Si-*s* contribution, are detached and confined in the energy range −11 to −8 eV. The pseudo gap seen for LaSiH is maintained and located at around −2 eV.

The electronic structures of $R\bar{3}m$ $LaSiH_6$ and *P*1 $LaSiH_7$ are rather easy to interpret. Occupied states relate to bonding and nonbonding molecular orbitals of the hypervalent SiH_6^{2-} ion, six per f.u.[64] For charge-imbalanced $LaSiH_6$ ($La^{3+}[SiH_6]^{2-}e$), these Si−H based bands are separated by a small gap from the conduction band (which has a large La contribution) and which hosts the additional electron, Figure 8c. For charge-balanced $LaSiH_7$, $La^{3+}[SiH_6]^{2-}(H^-)$, there is a sizable (≈3 eV) band gap at the Fermi level. The states of the hydridic H are largely confined in the narrow range between −4 and −2 eV, where also the nonbonding (e_g-type) states of the SiH_6^{2-} moiety are located, as shown in Figure 8d. The evolution of the electronic structure from the lower interstitial hydrides LaSiH and $LaSiH_2$ to the higher hydridosilicates is also clearly reflected in the Bader charge analysis (Table S7). The charge on Si changes from negative to positive, accompanied by a pronounced reduction in its Bader volume. In contrast, the charge on La increases slightly from approximately +1.5 to +1.8, while the hydrogen atoms carry charges in the range of −0.55 to −0.67.

Since LaSiH, $LaSiH_2$, and $LaSiH_6$ represent metals, it will be interesting to assess their superconducting properties. Figures S12 and S13 (showing the calculated phonon dispersion relations) also include phonon densities of states $F(\omega)$, Eliashberg electron−phonon coupling functions $\alpha^2F(\omega)$, and the cumulative electron−phonon coupling constants $\lambda(\omega)$. Values of the calculated superconductor parameters are presented in Table 2. LaSiH attains very low critical temperatures, below 1 K, whereas $LaSiH_2$ has a T_c in the range 9−11 K, slightly increasing with pressure, and $LaSiH_6$ has a T_c of 6 K at 0 GPa and about 9 K at 20 GPa, indicating a moderately strong electron-phonon coupling for both materials.

Table 2. Calculated Superconductor Parameters for *Cmcm* LaSiH, *Pnma* $LaSiH_2$, and $R\bar{3}m$ $LaSiH_6$. (λ = Electron-Phonon Coupling Constant, ω_{log} = Logarithmically Averaged Phonon Frequency, $DOS(E_F)$ = Number of States at the Fermi Level)

compound, *p*	λ	ω_{log}/meV	$DOS(E_F)$/eV^{-1}	T_c/K
Cmcm LaSiH, 0 GPa	0.28	27.0	1.07	0.8
Cmcm LaSiH, 20 GPa	0.21	34.8	0.87	0.3
Pnma $LaSiH_2$, 0 GPa	0.65	30.4	4.47	9.4
Pnma $LaSiH_2$, 20 GPa	0.61	37.9	4.11	11.1
$R\bar{3}m$ $LaSiH_6$, 0 GPa	0.54	30.1	1.21	5.0
$R\bar{3}m$ $LaSiH_6$, 20 GPa	0.54	45.0	1.10	7.3

4. CONCLUSIONS

The ternary systems La−Al−H and La−Si−H were investigated at pressures up to 20 GPa by computational structure prediction and *in situ* synchrotron diffraction studies. In the La−Al−H system, $LaAlH_6$ is the only stable ternary compound for 0 and 20 GPa predicted by CSP and in the experiments conducted at 2 and up to 12 GPa. While already reported with the $R\bar{3}m$ structure ($BaSiF_6$ type), we find that $R\bar{3}$ is slightly more stable at ambient conditions and increasingly more stable with pressure.

More variability was found in the La−Si−H system. At ambient pressure, only LaSiH is thermodynamically stable, with its *Cmcm* structure slightly more favored than the *Pnma*. At 20 GPa, $LaSiH_2$ (*Pnma*) and the semiconducting hydridosilicate $LaSiH_7$ are additionally stable. $LaSiH_6$ was found to be potentially stable at finite *T* or as a metastable phase. Among the metals LaSiH, $LaSiH_2$, and $LaSiH_6$, the latter two are superconducting with a moderately strong e-ph coupling. Our calculations suggest that $LaSiH_2$ has a T_c of 9 K at 0 GPa and 11 K at 20 GPa, and $LaSiH_6$ has a T_c of 5 K at 0 GPa and 7 K at 20 GPa. While $LaSiH_6$ and $LaSiH_7$ could not

https://doi.org/10.1021/acs.inorgchem.5c05140
Inorg. Chem. XXXX, XXX, XXX−XXX

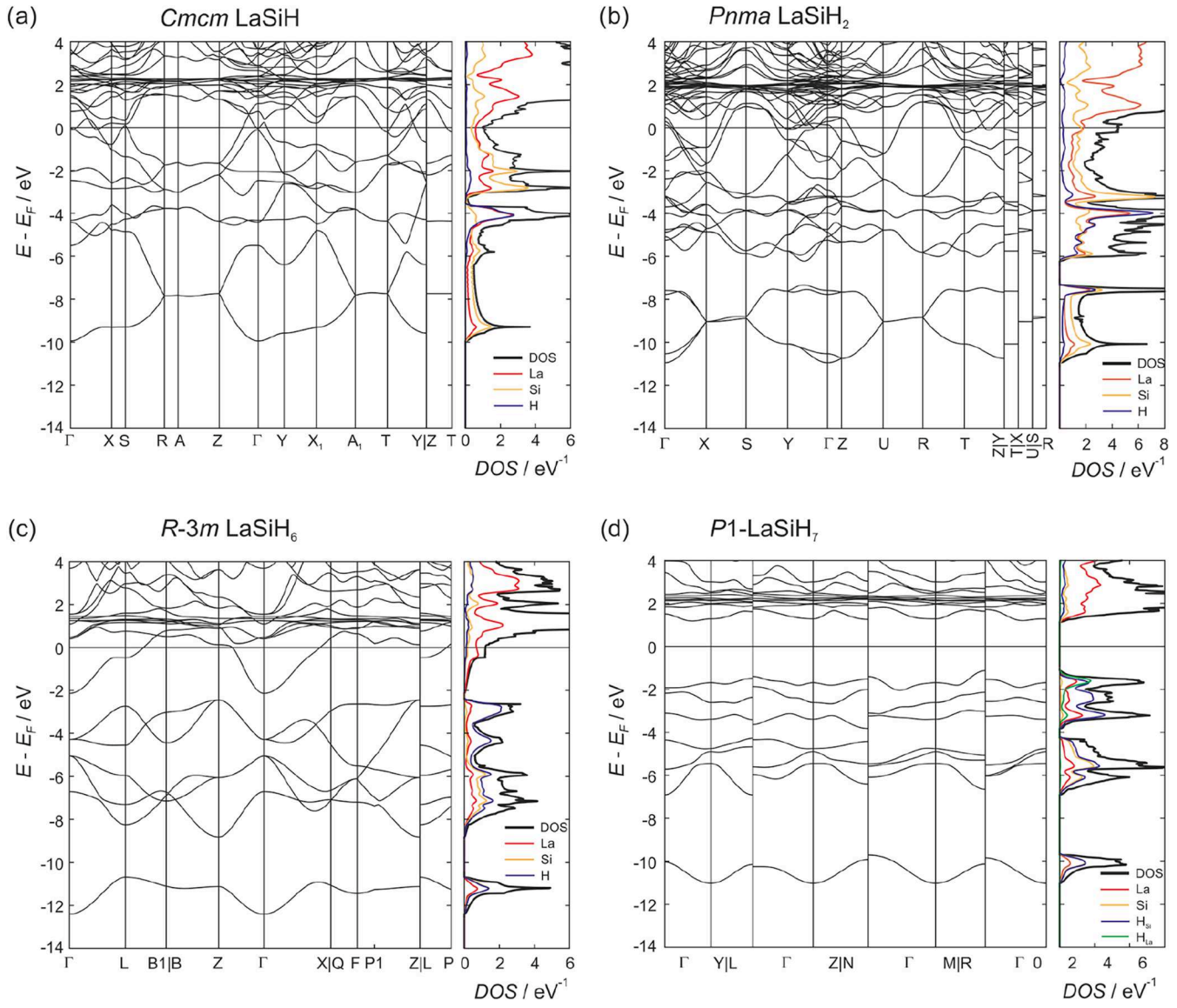

Figure 8. Electronic band structure and density of states (DOS) of *Cmcm* LaSiH (a), *Pnma* $LaSiH_2$ (b), $R\bar{3}m$ $LaSiH_6$ (c), and *P*1 $LaSiH_7$ (d) at their calculated equilibrium volumes (zero pressure). The DOS is partitioned into contributions of atoms. The H atoms of $LaSiH_7$ are divided between H atoms coordinated to Si (6) and the H atom exclusively coordinated to La (green line).

be observed experimentally, indications for a possible $LaSiH_2$ formation were present but could not be unambiguously confirmed. Simultaneous decomposition into LaH_3 and Si occurred, suggesting that pressures above 20 GPa and/or higher H_2 concentrations are necessary.

■ ASSOCIATED CONTENT

Supporting Information

The Supporting Information is available free of charge at https://pubs.acs.org/doi/10.1021/acs.inorgchem.5c05140.

Description of LaAl, LaSi, and $LaAl_{0.5}Si_{0.5}$ precursor characterization; DFT calculated enthalpy difference between $R\bar{3}m$ and $R\bar{3}$ $LaAlH_6$ as a function of pressure; DFT calculated enthalpy difference between *Cmcm* LaSiH and *Pnma* LaSiH as a function of pressure; *in situ* EDXRD patterns obtained during the hydrogenation of LaAl at 2 GPa; *in situ* EDXRD patterns obtained during the hydrogenation of $LaAl_{0.5}Si_{0.5}$ at 11 GPa; compilation of $LaAlH_6$ lattice parameters at various *p*, *T* conditions; *in situ* EDXRD patterns obtained during the hydrogenation of LaSi at 9 GPa; *ex situ* evaluation of product from the LaSi-H_2 experiment at 9 GPa; Le Bail fits for La_2AlSi-H_2, 11 GPa, 305 °C; LaSi-H_2, 9 GPa, 345 °C; LaSi-H_2, 20 GPa, 500 °C; DFT calculated *V*/*Z* vs pressure; phonon dispersion and electron−phonon coupling calculations for *Cmcm* LaSiH, *Pnma* $LaSiH_2$, $R\bar{3}m$ $LaSiH_6$, *P*1 $LaSiH_7$ at 0 and 20 GPa; DFT calculated structure data for $LaAlH_6$ and $LaSiH_n$ (n = 1,2,6,7); Bader charges and volumes for $LaSiH_n$ (n = 1,2,6,7) (PDF)

■ AUTHOR INFORMATION

Corresponding Author

Ulrich Häussermann − *Department of Chemistry, Stockholm University, 10691 Stockholm, Sweden;* orcid.org/0000-0003-2001-4410; Email: Ulrich.Häussermann@su.se

https://doi.org/10.1021/acs.inorgchem.5c05140
Inorg. Chem. XXXX, XXX, XXX−XXX

Authors

Doreen C. Beyer − *Institute of Inorganic Chemistry and Crystallography, Faculty of Chemistry, Leipzig University, D-04103 Leipzig, Germany*

Pedro Nunes Ferreira − *DEMAR, Escola de Engenharia de Lorena, Universidade de São Paulo, 12612-550 Lorena, Brazil; Institute of Theoretical and Computational Physics, Graz University of Technology, NAWI Graz, 8010 Graz, Austria;* orcid.org/0000-0002-1135-0570

Roman Lucrezi − *Department of Chemistry, Stockholm University, 10691 Stockholm, Sweden;* orcid.org/0000-0002-3117-3735

Luiz Tadeu Fernandes Eleno − *DEMAR, Escola de Engenharia de Lorena, Universidade de São Paulo, 12612-550 Lorena, Brazil*

Holger Kohlmann − *Institute of Inorganic Chemistry and Crystallography, Faculty of Chemistry, Leipzig University, D-04103 Leipzig, Germany;* orcid.org/0000-0002-8873-525X

Christoph Heil − *Institute of Theoretical and Computational Physics, Graz University of Technology, NAWI Graz, 8010 Graz, Austria;* orcid.org/0000-0001-9693-9183

Michael Sannemo Targama − *Department of Chemistry, Stockholm University, 10691 Stockholm, Sweden*

Volodymyr Baran − *Deutsches Elektronen-Synchrotron DESY, Notkestraße 85, D-22607 Hamburg, Germany;* orcid.org/0000-0003-2379-3632

Shrikant Bhat − *Deutsches Elektronen-Synchrotron DESY, Notkestraße 85, D-22607 Hamburg, Germany;* orcid.org/0000-0002-1229-9842

Robert Farla − *Deutsches Elektronen-Synchrotron DESY, Notkestraße 85, D-22607 Hamburg, Germany*

Kristina Spektor − *Deutsches Elektronen-Synchrotron DESY, Notkestraße 85, D-22607 Hamburg, Germany;* orcid.org/0000-0002-3267-9797

Complete contact information is available at: https://pubs.acs.org/10.1021/acs.inorgchem.5c05140

Notes

The authors declare no competing financial interest.

■ ACKNOWLEDGMENTS

This research has been supported by the Swedish Research Council (VR) through project 2019-06063, by the Deutsche Forschungsgemeinschaft (DFG, German Research Foundation) through project 277832266, and the Bundesministerium für Bildung und Forschung (BMBF)−German Federal Ministry of Education and Research through grant No. 05K20OLA. The P61B beamline LVP instrument has been funded through the ErUM-Pro program of the BMBF (grants nos.: 05K16WC2 & 05K13WC2). We are grateful to Per Mistenius for skillfully manufacturing the miniature press dies used for sample preparation. The computations were enabled by resources provided by the National Academic Infrastructure for Supercomputing in Sweden (NAISS), partially funded by the Swedish Research Council through grant agreement no. 2022-06725. DESY (Hamburg, Germany), a member of the Helmholtz Association HGF, is acknowledged for the provision of experimental facilities. Parts of this research were carried out at the PETRA III beamlines P61B and P02.1 through allocation of beamtime for proposals I-20220363 and I-20230157 as well as by an in-house contingent. RL acknowledges support from the Carl Tryggers foundation (CTS), grant no. 23:2934, and PNF acknowledges the São Paulo Research Foundation (FAPESP) under grants 2020/08258-0 and 2021/13441-1. PNF and CH acknowledge the computational resources of the dCluster of the Graz University of Technology and the VSC5 of the Austrian Scientific Computing (ASC) infrastructure.

■ REFERENCES

(1) Drozdov, A. P.; Kong, P. P.; Minkov, V. S.; Besedin, S. P.; Kuzovnikov, M. A.; Mozaffari, S.; Balicas, L.; Balakirev, F. F.; Graf, D. E.; Prakapenka, V. B.; Greenberg, E.; Knyazev, D. A.; Tkacz, M.; Eremets, M. I. Superconductivity at 250 K in lanthanum hydride under high pressures. *Nature* **2019**, *569* (7757), 528−531.

(2) Somayazulu, M.; Ahart, M.; Mishra, A. K.; Geballe, Z. M.; Baldini, M.; Meng, Y.; Struzhkin, V. V.; Hemley, R. J. Evidence for Superconductivity above 260 K in Lanthanum Superhydride at Megabar Pressures. *Phys. Rev. Lett.* **2019**, *122* (2), No. 27001.

(3) Peng, F.; Sun, Y.; Pickard, C. J.; Needs, R. J.; Wu, Q.; Ma, Y. Hydrogen Clathrate Structures in Rare Earth Hydrides at High Pressures: Possible Route to Room-Temperature Superconductivity. *Phys. Rev. Lett.* **2017**, *119* (10), No. 107001.

(4) Semenok, D. V.; Kvashnin, A. G.; Ivanova, A. G.; Svitlyk, V.; Fominski, V. Y.; Sadakov, A. V.; Sobolevskiy, O. A.; Pudalov, V. M.; Troyan, I. A.; Oganov, A. R. Superconductivity at 161 K in thorium hydride ThH10: Synthesis and properties. *Mater. Today* **2020**, *33*, 36−44.

(5) Kong, P.; Minkov, V. S.; Kuzovnikov, M. A.; Drozdov, A. P.; Besedin, S. P.; Mozaffari, S.; Balicas, L.; Balakirev, F. F.; Prakapenka, V. B.; Chariton, S.; Knyazev, D. A.; Greenberg, E.; Eremets, M. I. Superconductivity up to 243 K in the yttrium-hydrogen system under high pressure. *Nat. Commun.* **2021**, *12* (1), No. 5075.

(6) Chen, W.; Semenok, D. V.; Huang, X.; Shu, H.; Li, X.; Duan, D.; Cui, T.; Oganov, A. R. High-Temperature Superconducting Phases in Cerium Superhydride with a Tc up to 115 K below a Pressure of 1 Megabar. *Phys. Rev. Lett.* **2021**, *127* (11), No. 117001.

(7) Ma, L.; Wang, K.; Xie, Y.; Yang, X.; Wang, Y.; Zhou, M.; Liu, H.; Yu, X.; Zhao, Y.; Wang, H.; Liu, G.; Ma, Y. High-Temperature Superconducting Phase in Clathrate Calcium Hydride CaH6 up to 215 K at a Pressure of 172 GPa. *Phys. Rev. Lett.* **2022**, *128* (16), No. 167001.

(8) Eremets, M. I.; Minkov, V. S.; Drozdov, A. P.; Kong, P. P.; Ksenofontov, V.; Shylin, S. I.; Bud'ko, S. L.; Prozorov, R.; Balakirev, F. F.; Sun, D.; Mozaffari, S.; Balicas, L. High-Temperature Superconductivity in Hydrides: Experimental Evidence and Details. *J. Supercond. Nov. Magn.* **2022**, *35* (4), 965−977.

(9) Hirsch, J. E. Are hydrides under high-pressure-high-temperature superconductors? *Natl. Sci. Rev.* **2024**, *11* (7), No. nwad174.

(10) Semenok, D. V.; Zhou, Di.; Chen, W.; Kvashnin, A. G.; Sadakov, A. V.; Helm, T.; Ferreira, P. N.; Heil, C.; Pudalov, V. M.; Troyan, I. A.; Struzhkin, V. V. Stability and Superconductivity of Ternary Polyhydrides. *Ann. Phys.* **2025**, *538* (1), No. e00467.

(11) Zhang, Z.; Cui, T.; Hutcheon, M. J.; Shipley, A. M.; Song, H.; Du, M.; Kresin, V. Z.; Duan, D.; Pickard, C. J.; Yao, Y. Design Principles for High-Temperature Superconductors with a Hydrogen-Based Alloy Backbone at Moderate Pressure. *Phys. Rev. Lett.* **2022**, *128* (4), No. 47001.

(12) Hilleke, K. P.; Zurek, E. Rational Design of Superconducting Metal Hydrides via Chemical Pressure Tuning. *Angew. Chem., Int. Ed.* **2022**, *61* (38), No. e202207589.

(13) Di Cataldo, S.; Heil, C.; Linden, W. von der; Boeri, L. LaBH8: Towards high- Tc low-pressure superconductivity in ternary superhydrides. *Phys. Rev. B* **2021**, *104* (2), No. L020511.

(14) Lucrezi, R.; Di Cataldo, S.; Linden, W.; von der Boeri, L.; Heil, C. In-silico synthesis of lowest-pressure high-Tc ternary superhydrides. *npj Comput. Mater.* **2022**, *8* (1), No. 119.

(15) Flores-Livas, J. A.; Boeri, L.; Sanna, A.; Profeta, G.; Arita, R.; Eremets, M. A perspective on conventional high-temperature

superconductors at high pressure: Methods and materials. *Phys. Rep.* **2020**, *856*, 1−78.
(16) Song, Y.; Bi, J.; Nakamoto, Y.; Shimizu, K.; Liu, H.; Zou, B.; Liu, G.; Wang, H.; Ma, Y. Stoichiometric Ternary Superhydride LaBeH8 as a New Template for High-Temperature Superconductivity at 110 K under 80 GPa. *Phys. Rev. Lett.* **2023**, *130* (26), No. 266001.
(17) Song, X.; Hao, X.; Wei, X.; He, X.-L.; Liu, H.; Ma, L.; Liu, G.; Wang, H.; Niu, J.; Wang, S.; Qi, Y.; Liu, Z.; Hu, W.; Xu, B.; Wang, L.; Gao, G.; Tian, Y. Superconductivity above 105 K in Nonclathrate Ternary Lanthanum Borohydride below Megabar Pressure. *J. Am. Chem. Soc.* **2024**, *146* (20), 13797−13804.
(18) Saitoh, H.; Machida, A.; Aoki, K. Synchrotron X-ray diffraction techniques for in situ measurement of hydride formation under several gigapascals of hydrogen pressure. *Chin. Sci. Bull.* **2014**, *59* (36), 5290−5301.
(19) Parthé, E.; Hohnke, D.; Jeitschko, W.; Schob, O. Structure data of new intermetallic compounds. *Naturwissenschaften* **1965**, *52* (7), No. 155.
(20) Nylén, J.; Sato, T.; Soignard, E.; Yarger, J. L.; Stoyanov, E.; Häussermann, U. Thermal decomposition of ammonia borane at high pressures. *J. Chem. Phys.* **2009**, *131* (10), No. 104506.
(21) Spektor, K.; Crichton, W. A.; Filippov, S.; Klarbring, J.; Simak, S. I.; Fischer, A.; Häussermann, U. Na-Ni-H Phase Formation at High Pressures and High Temperatures: Hydrido Complexes NiH53- Versus the Perovskite NaNiH3. *ACS Omega* **2020**, *5* (15), 8730−8743.
(22) Spektor, K.; Crichton, W. A.; Filippov, S.; Simak, S. I.; Fischer, A.; Häussermann, U. Na3FeH7 and Na3CoH6: Hydrogen-Rich First-Row Transition Metal Hydrides from High Pressure Synthesis. *Inorg. Chem.* **2020**, *59* (22), 16467−16473.
(23) Vekilova, O. Y.; Beyer, D. C.; Bhat, S.; Farla, R.; Baran, V.; Simak, S. I.; Kohlmann, H.; Häussermann, U.; Spektor, K. Formation and Polymorphism of Semiconducting K2SiH6 and Strategy for Metallization. *Inorg. Chem.* **2023**, *62* (21), 8093−8100.
(24) Guignard, J.; Crichton, W. A. The large volume press facility at ID06 beamline of the European synchrotron radiation facility as a High Pressure-High Temperature deformation apparatus. *Rev. Sci. Instrum.* **2015**, *86* (8), No. 085112.
(25) SETO, Y.; Nishio-Hamane, D.; Nagai, T.; Sata, N. Development of a software suite on X-ray diffraction experiments. *Rev. High Press. Sci. Technol.* **2010**, *20*, 269−276.
(26) Le Bail, A.; Duroy, H.; Fourquet, J. L. Ab-initio structure determination of LiSbWO6 by X-ray powder diffraction. *Mater. Res. Bull.* **1988**, *23* (3), 447−452.
(27) Toby, B. H.; von Dreele, R. B. GSAS-II: the genesis of a modern open-source all purpose crystallography software package. *J. Appl. Crystallogr.* **2013**, *46* (2), 544−549.
(28) Matsui, M.; Higo, Y.; Okamoto, Y.; Irifune, T.; Funakoshi, K.-I. Simultaneous sound velocity and density measurements of NaCl at high temperatures and pressures: Application as a primary pressure standard. *Am. Mineral.* **2012**, *97* (10), 1670−1675.
(29) Dippel, A.-C.; Liermann, H.-P.; Delitz, J. T.; Walter, P.; Schulte-Schrepping, H.; Seeck, O. H.; Franz, H. Beamline P02.1 at PETRA III for high-resolution and high-energy powder diffraction. *J. Synchrotron Radiat.* **2015**, *22* (3), 675−687.
(30) Kieffer, J.; Wright, J. P. PyFAI: a Python library for high performance azimuthal integration on GPU. *Powder Diffr.* **2013**, *28* (S2), S339−S350.
(31) Boultif, A.; Louër, D. Indexing of powder diffraction patterns for low-symmetry lattices by the successive dichotomy method. *J. Appl. Crystallogr.* **1991**, *24* (6), 987−993.
(32) Taupin, D. A powder-diagram automatic-indexing routine. *J. Appl. Crystallogr.* **1973**, *6* (5), 380−385.
(33) Shirley, R. *Crysfire 2004: An interactive powder indexing support system* 2004.
(34) Rietveld, H. M. A profile refinement method for nuclear and magnetic structures. *J. Appl. Crystallogr.* **1969**, *2* (2), 65−71.
(35) Rodríguez-Carvajal, J. *FULLPROF (version 5.20):A Program for Rietveld Refinement and Pattern Matching Analysis*; Insitut Laue-Langevin: Grenoble (France), 2012.
(36) Korst, W. L.; Warf, J. C. Rare Earth-Hydrogen Systems. I. Structural and Thermodynamic Properties. *Inorg. Chem.* **1966**, *5* (10), 1719−1726.
(37) Oganov, A. R.; Glass, C. W. Crystal structure prediction using ab initio evolutionary techniques: principles and applications. *J. Chem. Phys.* **2006**, *124* (24), No. 244704.
(38) Glass, C. W.; Oganov, A. R.; Hansen, N. USPEX—Evolutionary crystal structure prediction. *Comput. Phys. Commun.* **2006**, *175* (11−12), 713−720.
(39) Kresse, G.; Furthmüller, J. Efficient iterative schemes for ab initio total-energy calculations using a plane-wave basis set. *Phys. Rev. B* **1996**, *54* (16), No. 11169.
(40) Kresse, G.; Furthmüller, J. Efficiency of ab-initio total energy calculations for metals and semiconductors using a plane-wave basis set. *Comput. Mater. Sci.* **1996**, *6* (1), 15−50.
(41) Kresse, G.; Joubert, D. From ultrasoft pseudopotentials to the projector augmented-wave method. *Phys. Rev. B* **1999**, *59* (3), No. 1758.
(42) Perdew, J. P.; Burke, K.; Ernzerhof, M. Generalized Gradient Approximation Made Simple. *Phys. Rev. Lett.* **1996**, *77* (18), No. 3865.
(43) Giannozzi, P.; Andreussi, O.; Brumme, T.; Bunau, O.; Buongiorno Nardelli, M.; Calandra, M.; Car, R.; Cavazzoni, C.; Ceresoli, D.; Cococcioni, M.; Colonna, N.; Carnimeo, I.; Dal Corso, A.; Gironcoli, S. de.; Delugas, P.; DiStasio, R. A.; Ferretti, A.; Floris, A.; Fratesi, G.; Fugallo, G.; Gebauer, R.; Gerstmann, U.; Giustino, F.; Gorni, T.; Jia, J.; Kawamura, M.; Ko, H.-Y.; Kokalj, A.; Küçükbenli, E.; Lazzeri, M.; Marsili, M.; Marzari, N.; Mauri, F.; Nguyen, N. L.; Nguyen, H.-V.; Otero-de-la-Roza, A.; Paulatto, L.; Poncé, S.; Rocca, D.; Sabatini, R.; Santra, B.; Schlipf, M.; Seitsonen, A. P.; Smogunov, A.; Timrov, I.; Thonhauser, T.; Umari, P.; Vast, N.; Wu, X.; Baroni, S. Advanced capabilities for materials modelling with Quantum ESPRESSO. *J. Phys.: Condens. Matter* **2017**, *29* (46), No. 465901.
(44) Giannozzi, P.; Baroni, S.; Bonini, N.; Calandra, M.; Car, R.; Cavazzoni, C.; Ceresoli, D.; Chiarotti, G. L.; Cococcioni, M.; Dabo, I.; Dal Corso, A.; Gironcoli, S. de.; Fabris, S.; Fratesi, G.; Gebauer, R.; Gerstmann, U.; Gougoussis, C.; Kokalj, A.; Lazzeri, M.; Martin-Samos, L.; Marzari, N.; Mauri, F.; Mazzarello, R.; Paolini, S.; Pasquarello, A.; Paulatto, L.; Sbraccia, C.; Scandolo, S.; Sclauzero, G.; Seitsonen, A. P.; Smogunov, A.; Umari, P.; Wentzcovitch, R. M. QUANTUM ESPRESSO: a modular and open-source software project for quantum simulations of materials. *J. Phys.: Condens. Matter* **2009**, *21* (39), No. 395502.
(45) Giannozzi, P.; Baseggio, O.; Bonfà, P.; Brunato, D.; Car, R.; Carnimeo, I.; Cavazzoni, C.; Gironcoli, S. de.; Delugas, P.; Ruffino, F. F.; Ferretti, A.; Marzari, N.; Timrov, I.; Urru, A.; Baroni, S. Quantum ESPRESSO toward the exascale. *J. Chem. Phys.* **2020**, *152* (15), No. 154105.
(46) Hamann, D. R. Optimized norm-conserving Vanderbilt pseudopotentials. *Phys. Rev. B* **2013**, *88* (8), 85117.
(47) Baroni, S.; de Gironcoli, S.; Dal Corso, A.; Giannozzi, P. Phonons and related crystal properties from density-functional perturbation theory. *Rev. Mod. Phys.* **2001**, *73* (2), No. 515.
(48) Schlipf, M.; Gygi, F. Optimization algorithm for the generation of ONCV pseudopotentials. *Comput. Phys. Commun.* **2015**, *196*, 36−44.
(49) Methfessel, M.; Paxton, A. T. High-precision sampling for Brillouin-zone integration in metals. *Phys. Rev. B* **1989**, *40* (6), No. 3616.
(50) Henkelman, G.; Arnaldsson, A.; Jónsson, H. A fast and robust algorithm for Bader decomposition of charge density. *Comput. Mater. Sci.* **2006**, *36* (3), 354−360.
(51) Sanville, E.; Kenny, S. D.; Smith, R.; Henkelman, G. Improved grid-based algorithm for Bader charge allocation. *J. Comput. Chem.* **2007**, *28* (5), 899−908.

https://doi.org/10.1021/acs.inorgchem.5c05140
Inorg. Chem. XXXX, XXX, XXX−XXX

(52) Tang, W.; Sanville, E.; Henkelman, G. A grid-based Bader analysis algorithm without lattice bias. *J. Phys.: Condens. Matter* **2009**, *21* (8), No. 84204.
(53) Bader, R. F. W. *Atoms in Molecules: A Quantum Theory*; Oxford University Press, 1990.
(54) Kresse, G.; Joubert, D. From ultrasoft pseudopotentials to the projector augmented-wave method. *Phys. Rev. B* **1999**, *59* (3), No. 1758.
(55) Dal Corso, A. Pseudopotentials periodic table: From H to Pu. *Comput. Mater. Sci.* **2014**, *95*, 337−350.
(56) Kogler, E.; Spath, D.; Lucrezi, R.; Mori, H.; Zhu, Z.; Li, Z.; Margine, E. R.; Heil, C. IsoME: Streamlining high-precision Eliashberg calculations. *Comput. Phys. Commun.* **2025**, *315*, No. 109720.
(57) Morel, P.; Anderson, P. W. Calculation of the Superconducting State Parameters with Retarded Electron-Phonon Interaction. *Phys. Rev.* **1962**, *125* (4), No. 1263.
(58) Weidenthaler, C.; Pommerin, A.; Felderhoff, M.; Sun, W.; Wolverton, C.; Bogdanović, B.; Schüth, F. Complex rare-earth aluminum hydrides: mechanochemical preparation, crystal structure and potential for hydrogen storage. *J. Am. Chem. Soc.* **2009**, *131* (46), 16735−16743.
(59) Chen, S.; Qian, Y.; Huang, X.; Chen, W.; Guo, J.; Zhang, K.; Zhang, J.; Yuan, H.; Cui, T. High-temperature superconductivity up to 223 K in the Al stabilized metastable hexagonal lanthanum superhydride. *Natl. Sci. Rev.* **2023**, *11* (1), No. nwad107.
(60) Bohmhammel, K.; Henneberg, E. Hydriding and dehydriding behavior of lanthanum silicides. *Solid State Ion.* **2001**, *141*−*142*, 599−602.
(61) Werwein, A.; Auer, H.; Kuske, L.; Kohlmann, H. From Metallic LnTt (Ln = La, Nd; Tt = Si, Ge, Sn) to Electron-precise Zintl Phase Hydrides LnTt H. *Z. Anorg. Allg. Chem.* **2018**, *644* (22), 1532−1539.
(62) Auer, H.; Guehne, R.; Bertmer, M.; Weber, S.; Wenderoth, P.; Hansen, T. C.; Haase, J.; Kohlmann, H. Hydrides of Alkaline Earth-Tetrel (AeTt) Zintl Phases: Covalent Tt-H Bonds from Silicon to Tin. *Inorg. Chem.* **2017**, *56* (3), 1061−1071.
(63) Sun, W.; Dacek, S. T.; Ong, S. P.; Hautier, G.; Jain, A.; Richards, W. D.; Gamst, A. C.; Persson, K. A.; Ceder, G. The thermodynamic scale of inorganic crystalline metastability. *Sci. Adv.* **2016**, *2* (11), No. e1600225.
(64) Puhakainen, K.; Benson, D.; Nylén, J.; Konar, S.; Stoyanov, E.; Leinenweber, K.; Häussermann, U. Hypervalent octahedral SiH6(2-) species from high-pressure synthesis. *Angew. Chem., Int. Ed.* **2012**, *51* (13), 3156−3160.
(65) Spektor, K.; Kohlmann, H.; Druzhbin, D.; Crichton, W. A.; Bhat, S.; Simak, S. I.; Vekilova, O. Y.; Häussermann, U. Hypervalent hydridosilicate in the Na-Si-H system. *Front. Chem.* **2023**, *11*, No. 1251774.
(66) Beyer, D. C.; Spektor, K.; Vekilova, O. Y.; Grins, J.; Carvalho, P. H. B. B.; Leinbach, L. J.; Sannemo-Targama, M.; Bhat, S.; Baran, V.; Etter, M.; Sano-Furukawa, A.; Hattori, T.; Kohlmann, H.; Simak, S. I.; Häussermann, U. Synthesis of BaSiH6 Hydridosilicate at High Pressures-A Bridge to BaSiH8 Polyhydride. *ACS Omega* **2025**, *10* (15), 15029−15035.
(67) Kubo, A.; Wang, Y.; Runge, C. E.; Uchida, T.; Kiefer, B.; Nishiyama, N.; Duffy, T. S. Melting curve of silicon to 15 GPa determined by two-dimensional angle-dispersive diffraction using a Kawai-type apparatus with X-ray transparent sintered diamond anvils. *J. Phys. Chem. Solids* **2008**, *69* (9), 2255−2260.

https://doi.org/10.1021/acs.inorgchem.5c05140
Inorg. Chem. XXXX, XXX, XXX−XXX